Inter-modal Raman amplification of OAM fiber modes

Rottwitt, Karsten; Koefoed, Jacob Gade; Ingerslev, Kasper; Kristensen, Poul

Published in:
APL Photonics

Link to article, DOI:
10.1063/1.5051794

Publication date:
2019

Document Version
Publisher's PDF, also known as Version of record

Inter-modal Raman amplification of OAM fiber modes

Cite as: APL Photonics **4**, 030802 (2019); https://doi.org/10.1063/1.5051794
Submitted: 13 August 2018 . Accepted: 31 January 2019 . Published Online: 27 February 2019

Karsten Rottwitt, Jacob Gade Koefoed, Kasper Ingerslev, and Poul Kristensen

Inter-modal Raman amplification of OAM fiber modes

Cite as: APL Photon. 4, 030802 (2019); doi: 10.1063/1.5051794
Submitted: 13 August 2018 • Accepted: 31 January 2019 •
Published Online: 27 February 2019

Karsten Rottwitt,[1,a)] Jacob Gade Koefoed,[1] Kasper Ingerslev,[1] and Poul Kristensen[2]

AFFILIATIONS

[1]DTU Fotonik, Ørsteds Plads, Building 343, 2800 Kongens Lyngby, Denmark
[2]OFS-Fitel, Priorparken 680, Brøndby 2605, Denmark

[a)]**Author to whom correspondence should be addressed:** karo@fotonik.dtu.dk

ABSTRACT

Raman scattering among conventional linearly polarized (LP) modes in single mode optical fibers is generally accepted as a promising way to achieve distributed amplification due to the fact that Raman amplification may provide gain at any wavelength, determined by the used pump wavelength, and excellent noise performance. Here, we show that Raman scattering among orbital angular momentum (OAM) modes in optical fibers have similar properties. We show theoretically that the Raman gain among OAM modes is independent on the topological charge of the OAM modes and that the gain efficiency when the pump and signal are parallel (orthogonally) polarized is similar to the Raman scattering among LP modes in parallel (orthogonal) states of polarization. In addition, we experimentally characterize Raman gain among OAM modes in a fiber supporting multiple OAM modes for both the pump and signal. Finally, we discuss the impact of polarization mode dispersion.

I. INTRODUCTION

Modes in optical fibers that carry orbital angular momentum (OAM) have recently received strong interest. Such modes have many interesting applications, for example, within high-resolution microscopy,[1] materials processing,[2] and quantum information science.[3] However, OAM modes have also been suggested as a key to address the everlasting need for more and more capacity in classical communication systems, a need that is currently pushing optical communication systems towards mode-division multiplexing. In this regard, applications of OAM modes hold great promise, especially when considering short range data transmission, for example, in datacenters. In such an application, one may explore the capability of OAM modes to carry data in the spatial dimension in addition to wavelength and time, while at the same time potentially eliminating the need for electrical signal processing, specifically multiple input-multiple output (MIMO) processing.[4] The latter may be achieved since OAM modes potentially have less mode coupling than other modes, for example, linearly polarized (LP) modes.[5,6]

The potential for using OAM modes in mode-division multiplexed optical communication has been demonstrated by several research groups. One of the pioneering system demonstrations was achieved by Bozinovic and co-workers in 2013, where transmission of 1.6 terabits per second, using two OAM modes and 10 wavelengths, through 1.1 km of fiber was achieved.[7] More recently, Ingerslev *et al.* demonstrated high capacity optical communication using as many as 12 OAM modes and 60 wavelengths per mode transmitted simultaneously, corresponding to a total aggregate capacity of 10.56 Tbit/s including forward error correction coding. The data were transmitted through 1.2 km of OAM fiber.[8] In relation to the maximum number of OAM modes guided by a fiber, as many as 36 OAM modes have been demonstrated by Brunet and co-workers in 2014.[9]

Without MIMO processing, the transmission distance of OAM modes has been limited to km-scale.[7] One reason for this is the lack of a fiber amplifier that can provide gain to OAM modes. However, erbium doped fiber amplifiers capable of amplifying OAM modes have been theoretically[10] and experimentally[11] researched. An alternative method is by the

use of Raman amplifiers, distributed as well as discrete. In 2017, Ingerslev and co-workers demonstrated Raman amplification in a fiber supporting 8 OAM modes.[12] The fiber length was constrained to 1.2 km. More recently, Long Zhu *et al.*[13] demonstrated a Raman amplifier providing gain over an 18 km OAM fiber. An on-off gain of about 3 dB for two OAM modes was shown.

Raman amplification for OAM modes has some fundamental benefits, such as simple amplifier architecture, broad gain bandwidth, flexible wavelength of operation, and low noise figure. In addition, since the intensity profiles of different OAM modes are very similar,[9] it is expected that Raman amplification exhibits only weak mode-dependence.

When considering the pump and signal in LP modes, guided by standard weekly guiding single mode fibers (SMFs), stimulated Raman scattering is conveniently described in terms of simple first order scalar differential equations in power or amplitude for the pump and signal. The description involves a scalar gain coefficient derived from the Raman susceptibility in a Cartesian coordinate system. To treat OAM modes using the same susceptibility requires solution of a vectorial problem. However, by translating the susceptibility to cyclic coordinates, the differential equations in power or amplitude again reduce to scalar equations.

As mentioned above, optical fibers that support stable propagation of OAM modes are different from SMFs. Suggested designs consist of an air core surrounded by a ring of relatively high refractive index compared to the cladding.[9,14] These fibers typically support not only a single OAM state but also multiple OAM states and superpositions of OAM states, or other beams with a singularity in the center, e.g., radially and azimuthally polarized modes, generally classified as vortex modes, and the fibers supporting such modes are referred to as vortex fibers.

In this paper, we provide a theoretical treatment of intermodal Raman scattering in Sec. II followed by an experimental characterization in Sec. III. The theoretical treatment focuses on a comparison between Raman scattering among vortex modes and Raman scattering among LP modes. More specifically, we focus on vortex modes, i.e., superpositions of two OAM modes with opposite topological charge, resulting in non-uniform polarization across the transverse plane of the beam, as opposed to modes where the polarization is uniform across the beam, i.e., beams formed on the basis of LP modes, as detailed in Sec. II A. For convenience, we refer to the latter modes as conventional modes. Starting from the coupled differential equations derived from Maxwell equations, we show in Sec. II B that the effective susceptibility and the effective Raman area are key when comparing intermodal Raman scattering among different modes. In Sec. II C, we evaluate the Raman effective area for various OAM modes, and in Sec. II D, we compare the effective Raman susceptibility for different modes with focus on cases where the pump and signal are in parallel and orthogonal states of polarization. The impact of polarization mode dispersion (PMD) on Raman amplifiers where the pump and signal propagate simultaneously has been analysed for the pump and signal in different states of polarization in SMFs.[15] Here, we discuss the impact of PMD in Raman amplifiers in vortex fibers, and finally, we show the susceptibility tensor in cyclic coordinates. In Sec. III, we compare the theoretical results against experimental data and confirm that a simple scalar approach may be used to predict the gain of a signal in an OAM mode being Raman amplified by a pump in an OAM mode and that the gain efficiency agrees with theoretical predictions. Finally, we compare the Raman gain among different combinations of pump and signal OAM states.

II. THEORY

In a conventional optical fiber, SMF, or multimode fiber, which supports propagation of LP modes, stimulated Raman scattering between a pump and a signal is described by a set of first order coupled differential equations. The coupling strength, i.e., the Raman gain coefficient, depends on the material as described through the material Raman susceptibility, and the spatial overlap between the intensity distribution of the pump and the signal, i.e., the effective Raman interaction area.[16] In germanosilicate glass based optical fibers, the symmetry of the Raman susceptibility tensor reflects that the Raman scattering depends on the relative polarization states of the pump and signal. Thus, to describe intermodal stimulated Raman scattering, we consider an electric field that consists of a superposition of two monochromatic vector fields, a pump, $\vec{E}_p$ at frequency ω_p, and a signal, $\vec{E}_s$, at frequency ω_s. The pump and signal propagate simultaneously in individual but arbitrary and possibly distinct modes guided by the optical fiber. Therefore, the composite electric field we consider is

$$\vec{E} = \frac{1}{2}\left\{\vec{E}_p e^{-i\omega_p t + i\beta_p z} + \vec{E}_s e^{-i\omega_s t + i\beta_s z} + \text{c.c.}\right\}, \tag{1}$$

where β_p and β_s are the propagation constants of the pump and signal, respectively, and c.c. is the complex conjugate. The pump and signal propagate along the z-axis, and it is valid to assume that $\vec{E}_p$ and $\vec{E}_s$ are in the xy-plane. To analyse the dependence on the transverse field distribution and the polarization state of the field, we write the amplitude of the fields at the pump and signal as

$$\vec{E}_j = A_j \frac{\vec{F}_j}{N_j}, \tag{2}$$

where A_j is a complex amplitude; here and in the following, we use index j to indicate the signal ($j = s$) or the pump ($j = p$). $\vec{F}_j$ is the vectorial electric transverse mode distribution, and N_j is a normalization factor which ensures that $|A_j|^2$ is the power in Watts carried by the electric field in the pump and signal, respectively. In our discussion of the mode dependency that follows, we write the vectorial electric transverse mode distribution, $\vec{F}_j$, in terms of a scalar radial field distribution $f_j(x, y)$ and a polarization unit vector $\hat{e}_j$, i.e., $\vec{F}_j = f_j(x, y)\hat{e}_j$.

In the following, we discuss stimulated Raman scattering among vortex beams and, in particular, OAM beams. In Sec. II A, we summarize the relevant properties of vortex beams with respect to Raman scattering, and in Sec. II B, we describe the propagation equation with emphasis on Raman scattering. Section II C focuses on the effective Raman area,

while Sec. II D focuses on the effective Raman susceptibility; its polarization dependence Sec. II D 1, the impact of PMD Sec. II D 2, and we show that by using a cyclic coordinate system Sec. II D 3, Raman gain among OAM states may be described using a single tensor element and a single propagation equation.

A. Modes

Before introducing a detailed theoretical description of the Raman interaction among modes, we start by summarizing the most importing properties of OAM modes as compared to the more conventional LP modes.

LP modes are characterized by two numbers: l and p. The number l quantifies the number of zero crossings of the field when going one full circle at a constant radius from the core. The number p quantifies the number of zero crossings of the field in the radial direction. If the z-component of the electric field may be neglected, for example, under the weakly guiding approximation, the electric field vector for a continuous wave (CW) is a two-dimensional vector

$$\vec{E} = \frac{1}{2}\frac{A}{N}\hat{e}f_{lp}(\vec{r}_\perp)e^{i\beta_{lp}z}e^{-i\omega t} + \text{c.c.}, \tag{3}$$

where A is the amplitude of the field, N is the normalization factor, $\hat{e}$ is the polarization vector, and $f_{lp}(\vec{r}_\perp)$ is the transverse envelope of the modes of the electric field, all introduced in Eq. (2). Each mode has a unique transverse field distribution identified by the sub-index "lp" that is a function of a point in the transverse plane ($\vec{r}_\perp = (x, y)$). β_{lp} is the propagation constant of mode lp.

The polarization vector, $\hat{e}$, is a two-dimensional column unit vector that describes the polarization state of the electric field, i.e., the Jones vector of the field. Here and in the following, "hat" $\hat{}$ denotes a unit vector. $\hat{e}$ may, for example, be a vector along the x axis or the y axis or for arbitrary but linear state of polarization $\hat{e} = [\cos(\phi)\ \sin(\phi)]^T$ or a circular state of polarization $\hat{e} = (1\sqrt{2})(1\ \pm i)^T$, the latter obtained, for example, by adding two cross polarized mode-degenerate LP modes with a $\pi/2$ phase shift. Any arbitrary state of polarization is obtained by combining two degenerate orthogonal LP modes with an appropriate phase difference. A characteristic of such a beam is that the polarization is spatially uniform across the transverse plane of the beam. Its state of polarization is commonly mapped onto a Poincare sphere (PS).[17]

OAM modes are characterized by three quantities:[6] (i) an optical angular momentum ($\ell\hbar$) per photon, where ℓ (= 0, ±1, ±2, ±3,...) is referred to as the topological charge, related to the phase front of the beam, more specifically the number of azimuthal phase windings about the propagation axis, (ii) a radial order (also referred to as the mode number), identical to the number of concentric intensity rings in the intensity profile of the beam, and (iii) a spin angular momentum of ($\pm\hbar$) per photon–positive: ($+\hbar$) for the left-polarization vector: $\hat{\sigma}^+ = (\hat{x} + i\hat{y})/\sqrt{2}$ and negative: ($-\hbar$) for the right-polarization vector: $\hat{\sigma}^- = (\hat{x} - i\hat{y})/\sqrt{2}$.

OAM modes are conveniently described by so-called aligned and anti-aligned modes.[6] A continuous wave in an aligned mode, for which spin and topological charges have the same sign, is described by

$$\vec{E}_V = \frac{1}{2}\frac{A}{N}f_{\ell m}(\vec{r}_\perp)\hat{\sigma}^\pm e^{\pm i|\ell|\phi}e^{i\beta_v z}e^{-i\omega t} + \text{c.c.}, \tag{4}$$

where A is the amplitude of the field, N is the normalization factor, $f_{\ell m}(\vec{r}_\perp)$ is the radial field distribution, $\vec{r}_\perp = (r, \phi)$ are the transverse spatial coordinates, and β_v is the propagation constant, similar to Eq. (3).

A continuous wave in an anti-aligned mode, where the spin and angular momentum have opposite signs, is described by

$$\vec{E}_W = \frac{1}{2}\frac{A}{N}f_{\ell m}(\vec{r}_\perp)\hat{\sigma}^\pm e^{\mp i|\ell|\phi}e^{i\beta_w z}e^{-i\omega t} + \text{c.c.}, \tag{5}$$

where A, N, $f_{\ell m}(\vec{r}_\perp)$, $\hat{\sigma}^\pm$, and β_w are defined in analogue to Eq. (4).

In circular cylindrical optical fibers, the aligned modes are based on a sum of two cross polarized degenerate HE modes added with a $\pi/2$ phase shift, whereas the anti-aligned modes are based on a sum of two cross polarized degenerate EH modes added with a $\pi/2$ phase shift.[6] The aligned and anti-aligned modes are in general slightly non-degenerate from each other, i.e., $\beta_w \neq \beta_v$.

The state of polarization of a vortex beam is described by a linear combination of two orthogonal OAM states with opposite topological charge, appropriate weight, and phase difference. More specifically, the polarization vector of a vortex beam is described by

$$\hat{e} = [\cos(\Theta/2)\exp(-i\Phi/2)]|L_\ell\rangle + [\sin(\Theta/2)\exp(i\Phi/2)]|R_\ell\rangle, \tag{6}$$

where Θ and Φ are the spherical coordinates on the so-called higher order Poincare sphere (HOPS) and $|L_\ell\rangle = e^{-i\ell\phi}|\hat{\sigma}^+\rangle$ and $|R_\ell\rangle = e^{i\ell\phi}|\hat{\sigma}^-\rangle$. It is noted that the basis vectors are the two OAM states corresponding to the poles on the HOPS ($\Theta = 0$) and ($\Theta = \pi$), respectively. As pointed out by Milione *et al.*,[18] it is necessary to differentiate between $\ell \geq 1$ and $\ell < 0$ ($\ell = 0$ represents a trivial case of no orbital angular momentum). For $\ell \geq 1$, the beams are referred to as general vector beams and on the equator of the HOPS, azimuthally polarized beams, (Θ, Φ, ℓ) = ($\pi/2$, π, 1), and radially polarized beams, (Θ, Φ, ℓ) = ($\pi/2$, 0, 1), are found.[18–20] For $\ell < 0$, the beams are referred to as π-vector beams and on the equator of the HOPS, π-azimuthally polarized beams, (Θ, Φ, ℓ) = ($\pi/2$, π, –1), and π-radially polarized beams, (Θ, Φ, ℓ) = ($\pi/2$, 0, –1), are found.[18]

B. Propagation equations

With the above definitions of the pump and signal fields, one may now derive coupled propagation equations for the pump and signal, starting from Maxwell equations.[21,22] The resulting propagation equations are

$$\frac{dA_p}{dz} = \frac{i\omega_p e^{-i\beta_p z}}{4N_p}\int_S \vec{F}_p^* \cdot \vec{P}_{\omega_p}^{NL} ds - \frac{\alpha_p}{2}A_p \tag{7}$$

for the amplitude of the pump and

$$\frac{dA_s}{dz} = \frac{i\omega_s e^{-i\beta_s z}}{4N_s}\int_S \vec{F}_s^* \cdot \vec{P}_{\omega_s}^{NL} ds - \frac{\alpha_s}{2}A_s \tag{8}$$

for the amplitude of the signal. The vector $\vec{P}_{\omega_p}$ ($\vec{P}_{\omega_s}$) is the nonlinear induced polarization at the frequency of the pump (signal). The normalization factor for the pump and signal is evaluated to be

$$N_j^2 = \frac{c\varepsilon_0 n_j^{eff}}{2}\int_S |\vec{F}_j|^2 ds, \tag{9}$$

where n_j^{eff} is the effective refractive index of the pump ($j = p$), respectively, the signal ($j = s$). The intrinsic attenuation of the pump and signal is included through α_p and α_s, and the other parameters are as defined earlier. Note that due to the vectorial representation, these equations are valid independent on the choice of the coordinate system.

The induced polarization at the signal frequency ω_s is related to the material susceptibility and the electric field through

$$\vec{P}_{\omega_s} = \varepsilon_0 \frac{3}{2}\begin{pmatrix} p_{11} & p_{12} \\ p_{11} & p_{22}\end{pmatrix}\cdot \vec{E}_s, \tag{10}$$

where ε_0 is the vacuum permittivity, the factor $(3/2)$ takes into account the intrinsic permutation symmetry of the susceptibility tensor, and

$$p_{11} = \chi_{xxxx}|E_x^p|^2 + \chi_{xxyy}|E_y^p|^2, \tag{11}$$

$$p_{12} = \chi_{xyyx}E_y^p(E_x^p)^* + \chi_{xyxy}E_x^p(E_y^p)^*, \tag{12}$$

$$p_{21} = \chi_{yxxy}E_x^p(E_y^p)^* + \chi_{yxyx}E_y^p(E_x^p)^*, \tag{13}$$

$$p_{21} = \chi_{yyyy}|E_y^p|^2 + \chi_{yyxx}|E_x^p|^2, \tag{14}$$

where χ_{ijkl} are the susceptibility tensor elements, and, finally, E_i^p is the ith-component of $\vec{E}^p$ and similarly for E_i^s.[23]

By using $\vec{F}_j = f_j\hat{e}_j$, for the transverse part of the electric field as introduced in Eq. (2), we obtain the vector product of the transverse mode vector and the induced polarization at the signal frequency in Eq. (8)

$$\vec{F}_s^* \cdot \vec{P}_{\omega_s}^{NL} = |f_s|^2 \frac{A_s}{N_s}\left|f_p\frac{A_p}{N_p}\right|^2 \varepsilon_0 \frac{3}{2}\chi_{eff}, \tag{15}$$

where we have introduced the effective susceptibility χ_{eff} as[23]

$$\chi_{eff} = \hat{e}_s^* \cdot \begin{pmatrix} c_1 \\ c_2\end{pmatrix}, \tag{16}$$

where

$$c_1 = (\chi_{xxxx}|e_x^p|^2 + \chi_{xxyy}|e_y^p|^2)e_x^s + (\chi_{xyyx}e_y^p(e_x^p)^* + \chi_{xyxy}e_x^p(e_y^p)^*)e_y^s, \tag{17}$$

$$c_2 = (\chi_{yxxy}e_x^p(e_y^p)^* + \chi_{yxyx}e_y^p(e_x^p)^*)e_x^s + (\chi_{yyyy}|e_y^p|^2 + \chi_{yyxx}|e_x^p|^2)e_y^s. \tag{18}$$

It is noted that, for each tensor element, the sub-index is associated with a frequency, specifically χ_{ijkl} $(-\omega_s; \omega_s, \omega_p, -\omega_p)$. However, to keep the notation short, the frequency arguments are skipped here and in the following.

Assuming that there is no pump depletion, the solution to the propagation equation (8) is

$$A_s(z) = A_s(z=0)\exp\left[\frac{i3\omega_s}{2c^2\varepsilon_0 n_p n_s}\frac{\chi_{eff}}{A_{eff}^{ps}}P_L L_{eff} - \frac{\alpha_s}{2}L\right], \tag{19}$$

where P_L is the launched pump power and where we have included the intrinsic fiber attenuation of the pump through the effective length ($L_{eff} = (1 - e^{-\alpha_p L})/\alpha_p$), where α_p (α_s) is the attenuation rate of the pump (signal) mode, as introduced in Eq. (7) [Eq. (8)], and L is the physical length of the fiber. Finally, the Raman effective area A_{eff}^{ps} equals

$$A_{eff}^{ps} = \frac{\int |f_p|^2 ds \int |f_s|^2 ds}{\int |f_p|^2 |f_s|^2 ds}. \tag{20}$$

The superscript index (ps) to the effective area is used to differentiate the Raman effective area from the standard self-phase modulation area used when describing the nonlinear refractive index.[24] To arrive at Eq. (19), it has furthermore been assumed that the susceptibility is constant throughout the region where the electric field is significant. Hence, integrals that have the form $\int \chi_{ijkl}|f_p|^2|f_s|^2 ds$ reduces to $\chi_{ijkl}\int |f_p|^2|f_s|^2 ds$.

From the above, it is clear that the Raman gain is determined by the Raman effective area which is an overlap integral between the intensities of the interacting fields and the effective susceptibility. This also holds for any fields and modes including OAM states, and consequently, we discuss the Raman effective area and the effective Raman susceptibility in the following.

C. The Raman effective area

The Raman effective area of OAM modes is naturally determined by the fiber design. In the following, we consider a fiber designed to support 8 different OAM modes[6,12] with $|\ell| = 5$ and $|\ell| = 7$ each with right and left circular polarization, i.e., $\hat{\sigma}^{\pm}$. The fiber is based on an air core surrounded by a ring of higher refractive index than the cladding. The mode size of OAM modes is in general larger than the mode size of LP modes, and it is thus expected that the Raman effective area is larger than the Raman effective area of LP modes guided by SMFs, which is around 80 $(\mu m)^2$. Figure 1 shows the measured intensity plots of the modes of the transverse intensity profile.

Based on Eq. (20), we predict the Raman effective area, shown in Fig. 2. Fig. 2 shows four pump modes, given by two values of the topological charge ($\ell = 5$, $\ell = 7$) and for both right and left circular polarizations, i.e., $\sigma^{\pm}$. In Fig. 2 and the following text, the four modes are referred to as 5a for ($\ell = 5, \sigma^+$) and 7a for ($\ell = 7, \sigma^+$) for the two aligned modes and correspondingly for the anti-aligned modes: 5aa for ($\ell = 5, \sigma^-$) and 7aa for ($\ell = 7, \sigma^-$). The Raman effective area is only predicted for positive values of the topological charge, since the intensity distribution is identical for similar negative topological charges. In Fig. 2, and the following discussion, the notation

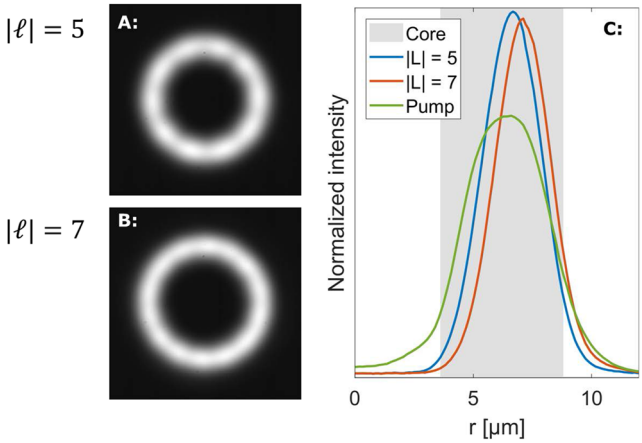

FIG. 1. (a) and (b) show two measured intensity distributions of $|\ell| = 5$ and $|\ell| = 7$ modes. (c) shows the intensity profile of the two modes and the profile of a pump distributed equally among all guided pump modes. The gray shaded area indicates the ring core of the fiber.

(sm, pm) refers to a set of signal-mode (sm) and pump-mode (pm).

From Fig. 2, it is clear that the Raman effective area is lowest for the pump and signal in similar modes; predicted effective area values (sm, pm) = (5a, 5a) of 156 μm^2 and (sm, pm) = (7a, 7a) = 158 μm^2. The Raman effective area between dissimilar modes having the same topological charge, and same radial order, but aligned versus anti-aligned modes, e.g., (sm, pm) = (5a, 5aa), depends only on the overlap between radial distributions as in Eq. (20). Consequently, such dissimilar modes exhibit a small Raman effective area. The Raman effective area between dissimilar modes (sm, pm) = (7a, 5a) equals 165 μm^2 and between (sm, pm) = (5a, 7a) the Raman effective area

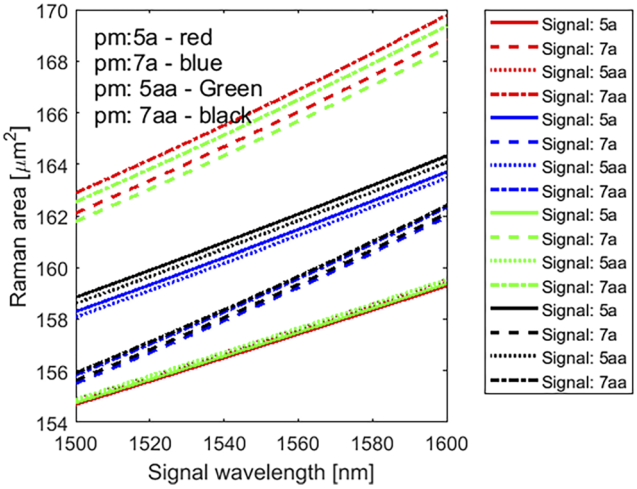

FIG. 2. Raman effective area versus signal wavelength. "pm" refers to the pump mode, the legend to the right provides the signal mode. The frequency of the pump is always 13 THz higher than the frequency of the signal wavelength.

equals 160 μm^2. These numbers may be compared against the effective Raman areas of SMFs of approximately 80 $(\mu m)^2$. Thus, from this, it is expected that the Raman gain coefficient is approximately half of what it is in more conventional SMFs of around 0.7 (W km)$^{-1}$ when the pump or signal is un-polarized.

D. The effective Raman susceptibility

Raman gain in SMF's is known to be polarization dependent. If the polarization state of the pump as well as the signal remain unchanged during propagation, the Raman gain is strongest if the pump and signal are in parallel states of polarization and weakest if the pump and signal are in orthogonal states of polarization. However, because of, for example, PMD, and the fact that the pump and signal are separated significantly in wavelength space, the polarization dependence may be mitigated, if the fiber is sufficiently long. We return to this mitigation later in this section. However, first, we discuss the polarization dependence, ignoring all propagation effects.

The polarization effects are described through the susceptibility tensor of the material by Eq. (16). Due to the spatial symmetry of amorphous germanium-codoped silicate glass, i.e., the host material of the optical fibers considered here, the susceptibility may be expressed conveniently through only two scalar functions A_Ω and B_Ω[25]

$$\chi_{iiii} = (A_\Omega + B_\Omega), \quad \chi_{ijij} = A_\Omega,$$
$$\chi_{iijj} = B_\Omega/2 \quad , \quad \chi_{ijji} = B_\Omega/2.$$

The two functions A_Ω and B_Ω are both functions of the difference in frequency between the pump and signal frequency, indicated by subindex Ω, and both are directly measurable through Raman scattering. By measuring the Raman gain coefficient when the pump and signal are linearly co-polarized, $(A_\Omega + B_\Omega)$ is determined, whereas B_Ω is measured by having the pump and signal in linearly orthogonally polarized modes.[15,26] The achievable Raman gain when the pump and signal are in perpendicular states of polarizations is more than an order of magnitude smaller than the gain when the pump and signal are in parallel states of polarizations, at pump-signal wavelength separations of interest in Raman amplifiers, i.e., when the signal frequency is shifted by 13 THz from the frequency of the pump ($A_\Omega \gg B_\Omega$ for $\Omega \approx 13$ THz). In typical long non-polarization maintaining fibers, the Raman gain assumes an average value of half of the gain when the pump and signal are parallel polarized.

For the purpose of comparing Raman scattering among modes guided by SMFs, i.e., conventional modes and fibers supporting propagation of vortex modes and, in particular, OAM modes, we calculate below the effective susceptibility for the Raman interaction among various vortex modes and, in particular, OAM states.

1. Polarization dependence

Below we consider two cases: case (a)—pump and signal in parallel states of polarization and case (b)—pump and signal in orthogonal states of polarization. The results are summarized in Table I.

TABLE I. Effective Raman susceptibility for various pump and signal mode combinations. Note: "pol." refers to polarization.

Conventional modes	Vortex modes	χ_{eff}
Case (a) parallel		
Both linearly pol.	Both radially (π-radially) or azimuthally (π-azimuthally):	$(A_\Omega + B_\Omega)$
Both circularly pol.	Both OAM	$(A_\Omega + B_\Omega/2)$
Case (b) orthogonal		
Both linearly pol.	One radially (π-radially) one azimuthally (π-azimuthally):	$B_\Omega/2$
Both circularly pol.	Both OAM	B_Ω

Case (a)—parallel states of polarization: In SMFs, modes are naturally expressed through LP modes and the strongest Raman interaction is found when the pump and signal are in parallel states of polarization, $(\hat{e}_s, \hat{e}_p) = (\hat{\imath}, \hat{\imath})$, where $\hat{\imath} \in (\hat{x}, \hat{y})$. This gives an effective susceptibility of $A_\Omega + B_\Omega$. In the case of fibers supporting propagation of vortex modes, the strongest Raman interaction is also found when the pump and signal are in parallel states of polarization, that is, both radially polarized, i.e., $\hat{e}_j = \left(|R_{\ell_j}\rangle + |L_{\ell_j}\rangle\right)/\sqrt{2}$, $\ell_j = 1$, where $(j = s, p)$ or both azimuthally polarized $\hat{e}_j = \left(|R_{\ell_j}\rangle - |L_{\ell_j}\rangle\right)/\sqrt{2}$, $\ell_j = 1$, where $(j = s, p)$. In both of these scenarios, the effective induced susceptibility equals $A_\Omega + B_\Omega$. The same results are obtained when both the pump and signal are π-radially or both π-azimuthally polarized $(\hat{e}_s, \hat{e}_p) = ((|R_{\ell_s}\rangle \pm |L_{\ell_s}\rangle)/\sqrt{2}, \left(|R_{\ell_p}\rangle \pm |L_{\ell_p}\rangle\right)/\sqrt{2})$, $\ell_s = \ell_p = -1$.

Amplifying a circularly polarized signal using a circularly polarized pump, both with the same handedness and both propagating in SMFs, results in an effective Raman susceptibility of $A_\Omega + B_\Omega/2$. In a vortex fiber, this corresponds to amplifying a signal in an OAM state of given polarization using a pump in an OAM state with the same polarization, i.e., $(\hat{e}_s, \hat{e}_p) = \left(|R_{\ell_s}\rangle, |R_{\ell_p}\rangle\right)$ or $(\hat{e}_s, \hat{e}_p) = \left(|L_{\ell_s}\rangle, |L_{\ell_p}\rangle\right)$. In this case, the effective susceptibility also equals $A_\Omega + B_\Omega/2$. It is emphasized that this is independent of the topological charge of the pump and signal.

Case (b)—orthogonal states of polarization: When the pump and signal in SMFs are in orthogonal states of polarization, a minimum Raman interaction is found, e.g., when $(\hat{e}_s, \hat{e}_p) = (\hat{x}, \hat{y})$, or $(\hat{e}_s, \hat{e}_p) = (\hat{y}, \hat{x})$, an effective susceptibility of $B_\Omega/2$ is found. In terms of vortex modes, an effective susceptibility of $B_\Omega/2$ is also found if the pump (signal) is radially polarized, while the signal (pump) is azimuthally polarized $(\hat{e}_s, \hat{e}_p) = ((|R_{\ell_s}\rangle \mp |L_{\ell_s}\rangle)/\sqrt{2}, \left(|R_{\ell_p}\rangle \pm |L_{\ell_p}\rangle\right)/\sqrt{2})$, $\ell_s = \ell_p = 1$. The same results are obtained when the pump (signal) is π-radially polarized, while the signal (pump) is π-azimuthally polarized $(\hat{e}_s, \hat{e}_p) = ((|R_{\ell_s}\rangle \mp |L_{\ell_s}\rangle)/\sqrt{2}, \left(|R_{\ell_p}\rangle \pm |L_{\ell_p}\rangle\right)/\sqrt{2})$, $\ell_s = \ell_p = -1$.

Amplifying a circularly polarized signal in an SMF using a circularly polarized pump with the opposite handedness as the signal, then an effective susceptibility of B_Ω is found. Amplifying a signal in an OAM state, for example, $|R_{\ell_s}\rangle$, using a pump with orthogonal polarization, i.e., $|L_{\ell_p}\rangle$ also gives a minimum effective susceptibility of B_Ω. Note, similar to the case of pump and signal in parallel polarized OAM states and also for orthogonal polarized OAM states, the effective Raman susceptibility is independent of the topological charge.

As noted, radially (π-radially) and azimuthally (π-azimuthally) polarized light are special cases of superposition's of two OAM states, both with topological charge equal to +1 (and −1 for π-vector beams), and the effective susceptibility is independent on the sign of the topological charge. Considering the more general cases, i.e., in the parallel case: $(\hat{e}_s, \hat{e}_p) = ((|R_{\ell_s}\rangle \pm |L_{\ell_s}\rangle)/\sqrt{2}, \left(|R_{\ell_p}\rangle \pm |L_{\ell_p}\rangle\right)/\sqrt{2})$ gives an effective Raman susceptibility equal to $A_\Omega + B_\Omega$ for $\ell_s = \ell_p$ (positive for general vector beams and negative for π-vector beams). This is explained by the fact that at any spatial point, the pump and signal are parallel polarized. In the orthogonal cases: $(\hat{e}_s, \hat{e}_p) = ((|R_{\ell_s}\rangle \pm |L_{\ell_s}\rangle)/\sqrt{2}, \left(|R_{\ell_p}\rangle \mp |L_{\ell_p}\rangle\right)\sqrt{2})$, the effective susceptibility equals $B_\Omega/2$ for $\ell_s = \ell_p$ (again positive for general vector beams and negative for π-vector beams) since the pump and signal are orthogonally polarized at any spatial point on the beams. The effective susceptibility for the orthogonal cases is thus much smaller than the effective susceptibility for the parallel cases, since $A_\Omega \gg B_\Omega$, as discussed in Sec. II D.

When the topological charge of the pump differs from the topological charge of the signal ($\ell_s \neq \ell_p$) in any of the two cases, the effective susceptibility equals a simple average of the two scenarios, i.e., the effective susceptibility equals $(A_\Omega + 3B_\Omega/2)/2$. This is found by utilizing orthogonality of beams having different topological charges. It is noted that in this case, the Raman amplification is non-uniform across the mode, which can in principle induce mode and polarization coupling. The average gain is expected in systems where averaging occurs due to fast mode coupling.

As shown in Table I, it is also found that when the pump and signal have the same topological charge, then in all cases, the Raman interaction among vortex modes depends on the polarization and not on the topological charge.

2. Impact of PMD

As mentioned earlier, non-polarization maintaining fibers randomize the state of polarization as a beam propagates through the fiber, i.e., the polarization rotates and goes through all states of polarization during propagation. This is explained by PMD and has been extensively analyzed in SMFs and recently also been researched in fibers supporting propagation of vortex modes.[27] In a fiber Raman amplifier, where the gain is accumulated over long lengths (typically several kilometers), the consequence of PMD and the fact that the pump and signal are separated significantly (up to around 13 THz or ten to hundreds of nanometers) the Raman gain is reduced from its maximum value and similarly increased from its minimum value.[15]

Analogously, when considering fibers supporting vortex modes, the polarization states of modes also change along

TABLE II. Effective Raman susceptibility when allowing pump and signal polarization to rotate but locked to each other. "||" ("⊥") refers to parallel (orthogonal) states of polarization.

Pump and signal polarization		
Conventional modes	Vortex modes	χ_{eff}
(sm ∥ pm) any state on PS	(sm ∥ pm) any state on HOPS	$(A_\Omega + 5B_\Omega/6)$
(sm ⊥ pm) any point on PS	(sm ⊥ pm) any point on HOPS	$2B_\Omega/3$

propagation due to PMD. Table II shows the impact on Raman gain due to PMD when averaging over the HOPS.

Let us first discuss the limit of large polarization-mode coupling but low PMD. When the pump and signal are launched in parallel, but arbitrary states of polarization, and assuming that they remain parallel polarized during propagation, i.e., the state of polarization of the pump and signal undergoes the same changes during propagation, then the resulting effective Raman susceptibility equals $A_\Omega + 5B_\Omega/6$. If on the other hand, the pump and signal are launched in orthogonal, but arbitrary states of polarization, and again remain orthogonal yet changing, then the Raman interaction is $2B_\Omega/3$.

Finally, and more realistically, consider the case of large polarization-mode coupling and large PMD. In this scenario, both the states of polarization of the pump and signal rotate independently on the PS and the HOPS, respectively, corresponding to conventional modes and vortex modes, respectively. In both cases, we find that the effective susceptibility equals $A_\Omega/2 + 3B_\Omega/4$ independent of the topological charge. This is exactly the average of the above.

3. Cyclic coordinates

Raman scattering among LP modes is most conveniently described in a standard Cartesian basis $(\hat{x}, \hat{y}, \hat{z})$, whereas it is natural to describe Raman scattering among OAM modes in a cyclic basis $(\hat{\sigma}^+, \hat{\sigma}^-, \hat{z})$. In either coordinate system, the Raman effect is described using the simple first order differential equations [Eqs. (7) and (8)]. This scalar approach is justified if, for example, the polarization states of the pump and signal fields do not change along the fiber, or if the fiber length is sufficiently long to ensure that an average gain coefficient may be used or when making simple predictions of Raman amplification.

Here, our focus is on Raman amplification of a signal in an OAM state pumped by a pump in an OAM state, either the same OAM state or a different OAM state. From the above, we have seen that the Raman interactions in such cases are independent on the topological charge and only depend on the polarization $\hat{\sigma}^+$ or $\hat{\sigma}^-$. Thus, by transferring the Raman susceptibility to a cyclic coordinate system[28] with the basis vectors $(\hat{\sigma}^+, \hat{\sigma}^-, \hat{z})$ as opposed to $(\hat{x}, \hat{y}, \hat{z})$, the task of theoretically/numerically predicting amplification of OAM modes simplifies. In this basis, the inter-modal Raman scattering among OAM states is described by a single differential equation similar to Eq. (8) for the rate of change in the amplitude with the distance equal to a simpler expression involving only one tensor element identified from Eqs. (21)–(24). If, for example, the pump and signal are in parallel polarized OAM modes, the gain coefficient is χ_{iiii}, $i \in (R, L)$, or if the pump and signal are in are in orthogonal states of polarized OAM modes, the gain coefficient is simply described by χ_{iijj}, $(i, j) \in (R, L)$. It is emphasized that the Raman susceptibility is independent of the topological charge

$$\chi_{RRRR} = \frac{1}{2}(\chi^{(3)}_{xxxx} + \chi^{(3)}_{xxyy} + \chi^{(3)}_{xyxy} - \chi^{(3)}_{xyyx}) = A_\Omega + B_\Omega/2 \quad (= \chi_{LLLL}), \tag{21}$$

$$\chi_{RRLL} = \frac{1}{2}(\chi^{(3)}_{xxxx} + \chi^{(3)}_{xxyy} - \chi^{(3)}_{xyxy} + \chi^{(3)}_{xyyx}) = B_\Omega \quad (= \chi_{LLRR}), \tag{22}$$

$$\chi_{RLLR} = \frac{1}{2}(\chi^{(3)}_{xxxx} - \chi^{(3)}_{xyyx} - \chi^{(3)}_{xyxy} - \chi^{(3)}_{xxyy}), = 0 \quad (= \chi_{LRRL}), \tag{23}$$

$$\chi_{RLRL} = \frac{1}{2}(\chi^{(3)}_{xxxx} + \chi^{(3)}_{xyyx} + \chi^{(3)}_{xyxy} - \chi^{(3)}_{xxyy}) = A_\Omega + B_\Omega/2 \quad (= \chi_{LRLR}). \tag{24}$$

The gain among two OAM states with the same polarization is nearly identical to gain among two linear polarizations ($\chi_{xxxx} \approx \chi_{RRRR}$). This approximation is most valid when the pump and signal are separated close to the gain peak (13 THz) as compared with the pump and signal being close in wavelength space, since B_Ω is larger close to the pump than at the gain peak where $B_\Omega \approx 0$.[25]

On the other hand, the Raman gain is twice as strong if the pump and signal are in two orthogonal OAM states ($|R_\ell\rangle$, $|L_\ell\rangle$) as opposed to two orthogonally linearly polarized modes. Yet, in both cases, the Raman scattering is still orders of magnitude smaller among orthogonal polarizations compared against parallel polarizations.

III. EXPERIMENTAL CHARACTERIZATION

In Sec. II, we addressed the question how Raman amplification among OAM modes compare against Raman amplification among conventional modes, as currently used in high capacity communications systems. In the following, we address this question experimentally by characterizing the Raman efficiency, scaled by the appropriate effective area and the attenuation of the fiber. First, we characterize the fiber loss and then the Raman gain efficiency.

The fiber that we used was the same as considered in Sec. II, i.e., an air core fiber[12] that supports propagation of 8 different OAM modes $|\ell| = 5$ and $|\ell| = 7$ and the polarizations given by σ^+ and σ^-.

Figure 3 shows the measured loss of the modes used in the following. The loss at the wavelength ≈1572 nm (later to be used as signal wavelength) is close to 1.1 dB/km. The loss at the wavelength ≈1470 nm (later to be used as pump wavelength) is 3.5 dB/km for the OAM $|\ell| = 5$ mode corresponding to an effective length of 769 m and 2.5 dB/km for the OAM $|\ell| = 7$ mode, corresponding to an effective length of 867 m.

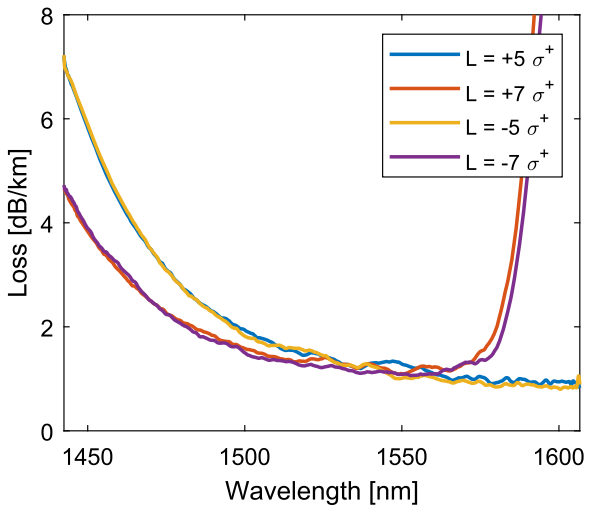

FIG. 3. Measured loss versus wavelength for four modes: two aligned $(\ell, \sigma) = (+5, \hat{\sigma}^+)$ and $(\ell, \sigma) = (+7, \hat{\sigma}^+)$ and for two anti-aligned $(\ell, \sigma) = (-5, \hat{\sigma}^+)$ and $(\ell, \sigma) = (-7, \hat{\sigma}^+)$. The physical length of the fiber was 1.2 km.

From Sec. II, it is expected that the Raman efficiency $(=g_r L_{eff})$ among OAM states, i.e., the Raman interaction between a pump in an OAM state and a signal also in an OAM state, is comparable to the Raman efficiency among LP modes only scaled in accordance with the effective area (Fig. 2) and the loss (Fig. 3). To verify this, we designed a well-calibrated experimental setup (see Fig. 4) to measure the Raman gain coefficient, i.e., the rate of change in gain in individual modes with the pump power also in individual modes.

In the experiment, a continuous wave (CW) external cavity laser (ECL) is used as a signal. Signal pulses are carved out from the CW signal using an external modulator (Mod). The signal is then launched into the OAM fiber, by using a spatial light modulator (SLM) and a quarter-wave plate, thus exciting a single OAM mode with a purity of at least 18 dB.

A pulsed pump beam is co-propagating with the signal. The pump beam is derived from another external cavity laser, also pulsed by using an external modulator. High pump power levels are achieved by the use of a thulium doped fiber amplifier. However, due to a mode dependent coupling loss, when coupling pump power to the fiber, a maximum pump power in the fiber equal to 4.7 W for the $|\ell| = 5$ modes and 3.5 W for the $|\ell| = 7$ was achieved. The mentioned power levels are peak power levels of the pump-pulses; however, the pump pulses are as a good approximation flat topped. A pulsed pump was chosen to give a maximum pump power. The duration of a signal pulse was 1 ns, while the duration of the pump pulse was 50 ns. These durations were chosen such that the signal in effect experience a CW pump.

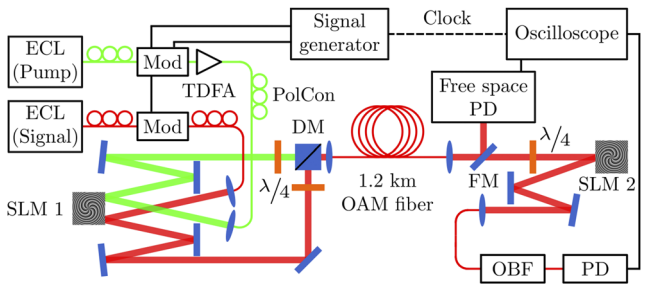

FIG. 4. Setup used to measure Raman gain. To obtain high pump power levels, we used a pulsed pump configuration, and consequently, the pump and signal are copropagating. Details are provided in the main text.

The wavelength of the pump was 1470 nm, while the wavelength of the signal was 1572 nm. This was chosen as a compromise between ensuring as low a loss of the pump as possible while at the same time also ensuring the lowest possible loss for the signal (see Fig. 3) and ensuring a frequency difference between the pump and signal close to 13 THz where germanium doped silica fibers have the strongest Raman interaction. At the output end of the fiber, the signal was separated from the pump using a dichroic mirror and a long pass filter, and the signal power was measured. By using two spatially separated points on the SLM, we were able to control specifically what modes were excited for the pump as well as for the signal.

By making a linear fit to the measured data for the on-off Raman gain, i.e., output signal power with the pump on relative to output signal power with the pump off, we obtained the curves illustrated in Fig. 5. From the slope of the on-off Raman gain with pump power, we obtained the Raman gain coefficient g_r by dividing the slope by the effective length for the respective pump modes times 4.3 $(= 10 \log e)$, $(dG_{dB}/dP_p = 4.3 g_r L_{eff})$. From this, the Raman gain coefficients listed in Fig. 5, all in units of $[(\text{W km})^{-1}]$, are found.

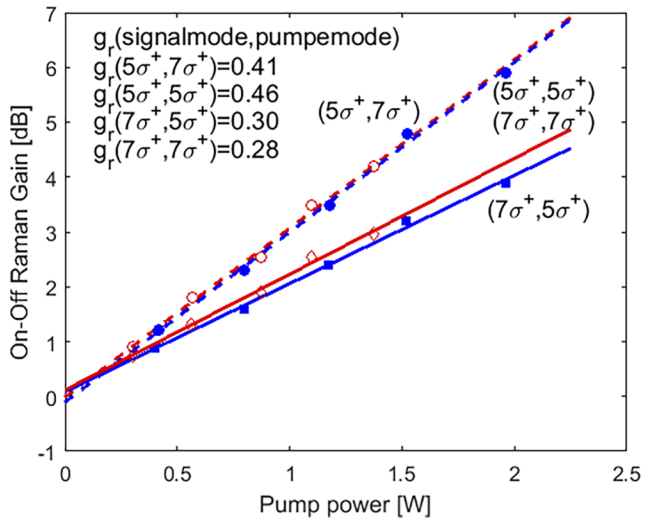

FIG. 5. On-off Raman gain versus pump power for four different combinations of signal and pump mode (sm, pm). Each curve is labeled with respective (sm, pm). Marks are measured data, whereas lines represent best fit and the slopes of the fit provides the value of the Raman gain coefficient, g_r (sm, pm), in $[(\text{W km})^{-1}]$.

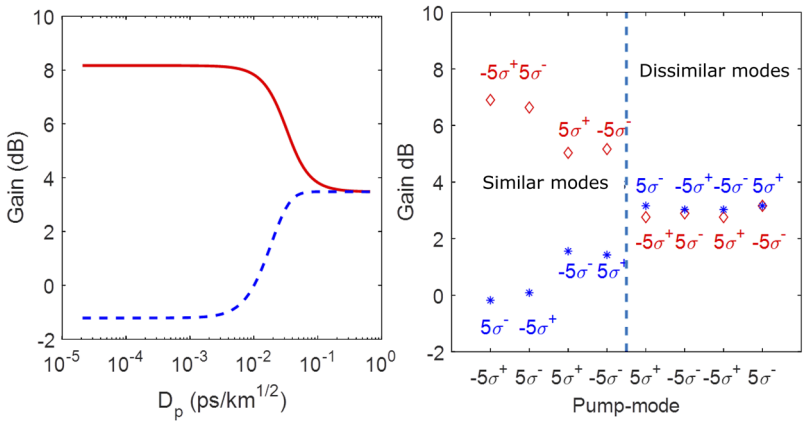

FIG. 6. Left: Predicted Raman gain versus PMD parameter, D_p, when the pump and signal are in parallel states of polarization (solid red curve) and orthogonal states of polarization (dashed blue curve). Parameters used: pump power—4 W, fiber length—1.2 km, attenuation—3.5 dB/km for the pump, 1.1 dB/km for the signal, Raman gain coefficients—0.7 $(\text{W km})^{-1}$ for parallel and 0.006 for orthogonal Right: Measured Raman gain between similar modes and dissimilar modes.

The gain coefficients listed in Fig. 5 should be compared against the Raman gain coefficients for single mode transmission fibers supporting propagation of LP modes. Such fibers have Raman gain coefficients of around 0.7 $(\text{W km})^{-1}$. However, due to the larger Raman effective area, discussed earlier, we expected a Raman gain coefficient reduced by approximately a factor of 2, i.e., to around 0.35 $(\text{W km})^{-1}$.

Combining data from Figs. 2 and 3, it is expected that the Raman efficiency of the modes (sm, pm) = (7a, 7a) is favourable over the (sm, pm) = (5a, 5a) modes. This is explained by the fact that even though the Raman effective area is lowest for the pump and signal in similar modes, (sm, pm) = (5a, 5a) of 156 μm^2 and (sm, pm) = (7a, 7a) of 158 μm^2 the difference in effective length $L_{eff}(|\ell| = 5) = 769$ m and $L_{eff}(|\ell| = 7) = 867$ m, make the Raman efficiency of the (sm, pm) = (7a, 7a) favourable over the (sm, pm) = (5a, 5a).

In addition, the dissimilar modes (sm, pm) = (7a, 5a) and (sm, pm) = (5a, 7a) have a larger Raman effective area compared against the Raman effective area between similar modes (sm, pm) = (5a, 5a) and (sm, pm) = (7a, 7a). However, the relatively low loss for the pump mode $|\ell| = 7$ compared to $|\ell| = 5$ make the Raman efficiency of the dissimilar modes (sm, pm) = (5a, 7a) comparable to the Raman efficiency of the similar modes (sm, pm) = (7a, 7a).

To examine the polarization dependence further, we selected a pump mode where the Raman effective area is expected to be the same when coupling to other modes. More specifically, from Fig. 2, by considering the pump in one of the aligned modes $(\ell, \hat{\sigma}) = (\pm 5, \hat{\sigma}^{\pm})$ or in one of the anti-aligned modes $(\ell, \hat{\sigma}) = (\pm 5, \hat{\sigma}^{\mp})$ and the signal in any of these four modes, then all cases are expected to have the nearly same effective area (Fig. 2) and the same effective length (Fig. 3). If the pump and signal propagate simultaneously without any change in their polarization state, then a significantly different gain would be expected when the pump and signal are parallel polarized as opposed to when the pump and signal are orthogonally polarized. However, as discussed above, since the polarization state of the pump and signal evolve differently throughout the 1.2 km fiber, an averaging is expected.

Using the method shown by Lin and Agrawal,[15] we predict that the gain for a signal polarized parallel to the pump is described by the solid line in Fig. 6, i.e., when there is no PMD, the pump and signal remain parallel polarized even though both move around on PS, i.e., they are locked together. Similarly, when the pump and signal are orthogonally polarized and remain orthogonally polarized during propagation, the lower trace in Fig. 6 is obtained. When the polarization state of the pump and signal evolve independently due to a large PMD, the pump and signal go through all states of polarization, an average gain is achieved with no dependence on the initial polarization state.

For comparison, we show in Fig. 6 (right) two sets of measured Raman gain; red marks when the pump and the signal have parallel polarization, while the blue marks when the pump and the signal have orthogonal polarization. The data are based on experimentally measured gain coefficients, from which we have extrapolated gain for pump values of 4 W. In addition, to the left of the dashed line, the pump and signal are in similar modes, i.e., (sm, pm) = (aligned, aligned) or (sm, pm) = (anti-aligned, anti-aligned), whereas to the right of the dashed line, the pump and signal are in dissimilar modes, i.e., (sm, pm) = (aligned, anti-aligned) or (sm, pm) = (anti-aligned, aligned).

Unfortunately, we have no experimental data for the PMD of the OAM fiber that we have used. However, adopting values from Ref. 27, a PMD coefficient from few hundredths of $\text{ps}/\sqrt{\text{km}}$ to tens of $\text{ps}/\sqrt{\text{km}}$ could exist in the fiber. Thus, from Fig. 6 (left), PMD could significantly impact our results and lead to PMD averaging of the Raman gain. Even though the data suggest that larger averaging happens when using dissimilar modes for the pump and signal than when using similar modes, we have only a few data points to support this conclusion.

IV. CONCLUSION

We have theoretically described the Raman interaction among vortex modes, with emphasis on orbital angular momentum (OAM) modes. In general, the Raman gain among any two modes scales linearly with the effective Raman susceptibility and inversely with the effective Raman area. We have shown that the Raman gain provided by an OAM mode to an OAM mode depends on the state of polarization but not on the topological charge. Parallel states give maximum

gain, whereas orthogonal states give order of magnitude less. We have analyzed the effective Raman susceptibility among radially and azimuthally polarized modes and shown that the Raman susceptibility between a pump and a signal both being radially or both being azimuthally polarized is identical to the effective Raman susceptibility between parallel linearly polarized modes, whereas the Raman susceptibility between a radially (azimuthally) polarized pump and an azimuthally (radially) polarized signal is identical to the Raman susceptibility between the orthogonal linearly polarized pump and signal. Similar results are found when replacing general vector modes with π-vector modes, i.e., radially and azimuthally polarized modes with π-radially and π-azimuthally polarized modes. For the purpose of theoretical predictions, we have evaluated the Raman susceptibility in a cyclic coordinate system, well suited to predict the Raman gain among OAM states. Finally, we have experimentally characterized the Raman gain in a vortex fiber supporting propagation of multiple OAM states. We have experimentally confirmed that the Raman scattering among the pump and signal in OAM states (parallel/orthogonally polarized) is equally strong as the Raman scattering among linearly polarized modes (parallel/orthogonally polarized), only scaled by the difference in effective Raman area. The impact of polarization mode dispersion on the Raman gain among vortex modes has been discussed.

ACKNOWLEDGMENTS

This research was financially supported, in part, by the Danish National Research Foundation Centre of Excellence SPOC (DNRF213) and the Danish Council for independent research under Grant No. DFF 4184-00433.

REFERENCES

[1]R. Chen, K. Agarwal, C. J. R. Sheppard, and X. Chen, Opt. Lett. **38**, 3111–3114 (2013).
[2]J. Hamazaki, R. Morita, K. Chujo, Y. Kobayashi, S. Tanda, and T. Omatsu, Opt. Express **18**, 2144 (2010).
[3]D. Cozzolino, D. Bacco, B. Da Lio, K. Ingerslev, Y. Ding, K. Dalgaard, P. Kristensen, M. Galili, K. Rottwitt, S. Ramachandran, and L. K. Oxenlnwe "Fiber-based high-dimensional quantum key distribution with twisted photons," in *CLEO Pacific Rim Conference 2018* (Optical Society America, 2018), Paper ID: Paper Th5A.
[4]A. Willner, H. Huang, Y. Yan, Y. Ren, N. Ahmed, G. Xie, C. Bao, L. Li, Y. Cao, J. Zhao, Z. Wang, M. Lavery, M. Tur, S. Ramachandran, A. Molisch, N. Ashrafi, and S. Ashrafi, Adv. Opt. Photonics **7**, 66 (2015).
[5]P. Gregg, P. Kristensen, and S. Ramachandran, Opt. Express **24**, 18938 (2016).
[6]P. Gregg, P. Kristensen, and S. Ramachandran, Optica **2**, 267 (2015).
[7]Y. Bozinovic, N. Yue, Y. Ren, M. Tur, P. Kristensen, H. Huang, A. Willner, and S. Ramachandran, Science **340**, 1545 (2013).
[8]K. Ingerslev, P. Gregg, M. Galili, F. Ros, H. Hu, H. Bao, M. A. U. Castaneda, P. Kristensen, A. Rubano, L. Marrucci, S. Ramachandran, K. Rottwitt, T. Morioka, and L. Oxenlwe, in Proceedings of OFC 2017, 2017, paper M2D 1.
[9]C. Brunet, P. Vaity, Y. Messaddeq, S. LaRochelle, and L. Rusch, Opt. Express **22**, 26117 (2014).
[10]J. Ma, F. Xia, S. Li, and J. Wang, in Proceedings of OFC 2015, 2015, paper W2A 40.
[11]J. Liu, H. Wang, S. Chen, S. Zheng, L. Zhu, A. Wang, N. Zhou, S. Li, L. Shen, C. Du, Q. Mo, and J. Wang, in Proceedings of OFC 2017, 2017, paper W2A 21.
[12]K. Ingerslev, P. Gregg, M. Galili, P. Kristensen, S. Ramachandran, K. Rottwitt, T. Morioka, and L. Oxenlwe, in Proceedings of CLEO Europe 2017, 2017.
[13]K. Zhu, J. Li, G. Zhu, L. Wang, C. Cai, A. Wang, S. Li, M. Tang, Z. He, S. Yu, C. Du, W. Luo, J. Liu, J. Du, and J. Wang, in Proceedings of OFC 2018, 2018, W4C 4.
[14]S. Ramachandran and P. Kristensen, Nanophotonics **2**, 455 (2013).
[15]Q. Lin and G. Agrawal, J. Opt. Soc. Am. B **20**, 1616 (2003).
[16]K. Rottwitt and J. H. Povlsen, J. Lightwave Technol. **23**, 3597 (2005).
[17]J. Damask, *Polarization Optics in Telecommunications* (Springer, 2005).
[18]G. Milione, H. Sztul, D. Nolan, and R. R. Alfano, Phys. Rev. Lett. **107**, 053601 (2011).
[19]G. Milione, S. Evans, D. Nolan, and R. R. Alfano, Phys. Rev. Lett. **108**, 190401 (2012).
[20]D. Naidoo, F. S. Roux, A. Dudley, I. Litvin, B. Piccirillo, L. Marrucci, and A. Forbes, Nat. Photonics **10**, 327 (2016).
[21]M. Kolesik and J. Moloney, Phys. Rev. E **70**, 036604 (2004).
[22]S. Friis, J. Koefoed, K. Guo, and K. Rottwitt, J. Opt. Soc. Am. B **35**, 702 (2018).
[23]K. Butcher and P. Cotter, *The Elements of Nonlinear Optics*, Cambridge Studies in Modern Optics 9 (Cambridge Univeristy Press, 1990).
[24]G. Agrawal, *Nonlinear Fiber Optics* (Academic Press, 2007).
[25]R. Hellwarth, Prog. Quantum Electron. **5**, 1 (1977).
[26]S. Trillo and S. Wabnitz, J. Opt. Soc. Am. B **9**, 1061 (1992).
[27]L. Wang, P. Vaity, S. Chatigny, Y. Messaddeq, L. A. Rusch, and S. LaRochelle, J. Lightwave Technol. **34**, 1661 (2016).
[28]K. Rottwitt and P. Tidemand-Lichtenberg, *Nonlinear Optics, Principles and Applications* (CRC Press, 2014).